Environmental
Science
Nano

ROYAL SOCIETY
OF CHEMISTRY

PAPER

View Article Online
View Journal | View Issue

Cite this: *Environ. Sci.: Nano*, 2023, **10**, 2754

The effect of kaolinite on ferrihydrite colloid migration in soil: molecular-scale mechanism study†

Lijuan Zeng,[a] Xiaofei Li,[b] Feng Jiang,[a] Meiling Yin,[a] Zhi Dang,[ac] Lijuan Zhang,[d] Weilin Huang[e] and Xiaoyun Yi*[a]

Received 25th May 2023,
Accepted 9th August 2023

DOI: 10.1039/d3en00333g

rsc.li/es-nano

The widespread ferrihydrite colloids in soil can carry diverse environmental contaminants, while current knowledge still remains lacking regarding the effects of the soil surface properties on migration behavior. Kaolinite (KL), a significant component of the porous media in aquifers, was used as a model material in experiments designed to explore its effect on the ferrihydrite colloid migration behavior. The experiments determined that KL caused a nearly 10-fold reduction in the mobility of ferrihydrite colloids. The decrease in travel distance of the colloids was primarily caused by the adsorption of ferrihydrite colloids on KL. The maximum ferrihydrite colloid adsorption capacity of KL was 20.2 mg g^{-1} at pH 5.5 and 5 mM $NaNO_3$ concentration. As confirmed by isothermal titration calorimetry, the inner-sphere complex formed between the ferrihydrite colloids and KL failed to cause the desorption of ferrihydrite colloids despite changes in pH or ionic strength. Density functional theory calculations and extended X-ray absorption fine structure spectroscopy analyses demonstrated that the ferrihydrite colloids coordinated to the KL surface by the formation of thermodynamically stable monodentate inner-sphere complexes with Al–O and Si–O active sites. To the best of our knowledge, this is the first investigation that describes the adsorption capacity of natural colloids by solid media, and studies their interaction mechanism in the molecular-scale. These new findings assist in the understanding of the migration behavior of ferrihydrite colloids in soil environments and provide a scientific basis for the prediction of contaminants' geochemical behavior in these environments.

Environmental significance

Ferrihydrite colloids commonly exist in soils and aquatic environments and their migration behaviors play a notable role in the fate of contaminants due to their unique activities. The interplay of ferrihydrite colloids with natural porous media highly influences the fate of ferrihydrite colloids and their associated contaminants. Kaolinite, as an important component of soil, is omnipresent in natural media. Therefore, it is of great environmental significance to discern the characteristics and influential mechanisms of kaolinite on the environmental behavior of ferrihydrite colloids. The present study quantitatively explored the adsorption behavior of ferrihydrite colloids on kaolinite, and clarify in depth the interfacial ferrihydrite colloid morphology on the exposed facets of kaolinite by batch adsorption experiments, isothermal titration calorimetry, extended X-ray absorption fine structure, and density functional theory calculations. The related findings provide a more thorough understanding of the migration of ferrihydrite colloids in natural environments, and extend our knowledge of the interactions between ferrihydrite and kaolinite.

1. Introduction

Colloids are ubiquitous in natural soil environments,[1,2] and have a strong adsorption effect on a variety of contaminants due to their micro to nanoscale size,[3,4] abundant adsorption sites, and high reactivity, thus playing a significant role in the fate and transport of multiple contaminants.[5–7] The influence of colloids on the migration behavior of contaminants varies notably, depending on the environmental behavior of the colloids.[8,9] Well-dispersed colloids in the soil solution exhibit a strong transport ability, promoting the migration of their associated contaminants,[10–12] while immobile colloids in

---

[a] *School of Environment and Energy, South China University of Technology, Guangzhou 510006, PR China. E-mail: xyyi@scut.edu.cn; Fax: +86 20 39380508; Tel: +86 20 39380508*

[b] *School of Environmental and Chemical Engineering, Foshan University, Foshan 528000, PR China*

[c] *The Key Lab of Pollution Control and Ecosystem Restoration in Industry Clusters, Ministry of Education, South China University of Technology, Guangzhou 510006, PR China*

[d] *School of Chemistry and Chemical Engineering, South China University of Technology, Guangzhou 510006, PR China*

[e] *Department of Environmental Sciences, Rutgers University, New Brunswick, NJ 08901, USA*

† Electronic supplementary information (ESI) available. See DOI: **https://doi.org/10.1039/d3en00333g**

solid soil media can retard the migration of contaminants that are adsorbed by the colloids.[9] The systematic understanding of the geochemical behavior of colloids is essential for assessing their potential in mobilizing or sequestering contaminants.

Sedimentation occurs when the colloids formed in soil becomes so large that they are immovable.[13] In addition, agglomeration also causes an increase in colloid size and is an important factor related to the formation of colloids that become immobile when they are trapped in porous media.[14] Recently many studies have found that the sedimentation and agglomeration of colloids depend greatly on the physicochemical characteristics of the aqueous solution, including fluid velocity, pH, and the presence of any coexisting ions.[6,15] In addition to the solution conditions, the properties of the solid surfaces also affect the colloid transport. Some models have shown that the inhibition of colloid migration increases with solid surface roughness.[16,17] Most previous studies have focused on the migration of colloids in columns of glass beads or quartz sand that were employed as models for naturally occurring transport solids, and show that those columns do not normally hinder the migration of well-dispersed colloids.[11,12,18] Nonetheless, natural porous media are composed of distinct mineral constituents with surface characteristics that are much more complicated than those of quartz sand or glass beads, and those characteristics have different effects on colloid transport.[19,20] In previous work, quartz sand has been coated with clays or iron oxide to simulate natural media in studies of the transport behavior of nanoparticles (*i.e.*, nanoscale zerovalent iron, nanoscale titanium dioxide, polystyrene nanoparticles, and graphene oxide).[19,21–23] The results have shown that the transport of nanoparticles is limited even when particle sizes are smaller than the pores in the media due to the electrostatic force between the nanoparticles and the media. However, the migration behavior of natural colloids that exist in soil, such as mineral colloids, is rarely studied in simulated natural media, and their complex interaction mechanisms remain unclear.

Iron is present in the earth's crust as the fourth most abundant element and the second most abundant metal.[24] The formation of ferrihydrite colloids from iron hydroxide precipitation is widespread in the natural environment.[25] Meanwhile, the ferrihydrite colloids, which exist widely in soils and aquatic environments, play a significant role in the fate of contaminants due to their unique activities.[26,27] Clay minerals are important soil components that are omnipresent in natural media, among which kaolinite (KL) is one of the most abundant types of clay minerals.[28,29] Therefore, it is necessary to discern the characteristics and influence mechanisms of KL on the environmental behavior of ferrihydrite colloids. It is of great significance to understand the behavior of colloids in the natural soil and sediment environments.

We speculated that there might be complicated interactive forces between mineral colloids and solid media. In fact, it has been suggested as early as 2012 that colloids might be deposited on solid soil media.[30] It was found that bulk iron oxide minerals (*e.g.*, goethite) are often cemented with KL as a binary association in soils, and that negatively charged functional groups on the surface of KL replaced the active hydroxyl groups on the surface of goethite ($\equiv$Al/Si–O– + HO–Fe$\equiv$ → $\equiv$Al/Si–O···Fe$\equiv$ + OH–).[31] A double-mononuclear Fe_2Si_2 structure can be formed by two Si tetrahedral groups connected with two Fe octahedra of ferrihydrite by a single Fe–O–Si bond.[32] To sum up, ferrihydrite colloids would also tend to adsorb onto KL during the migration process, and in addition to the electrostatic interaction, there may exist a complexing action that makes ferrihydrite colloids and KL bond more strongly. The mechanism of the influence of the interactions between media and colloidal functional groups on the migration behavior of colloids remains largely unknown.

The present study methodically investigates the cause and extent of the modulation effect of KL on the migration of ferrihydrite colloids *via* column experiments, batch adsorption experiments, isothermal titration calorimetry (ITC), extended X-ray absorption fine structure (EXAFS), and density functional theory (DFT) calculations. The objectives of this investigation are to (1) assess the mass transfer behavior of ferrihydrite colloids in sand coated with KL (KL-sand) to understand how KL affects the ferrihydrite colloid transport, (2) quantitatively study the adsorption behavior of ferrihydrite colloids on KL to reveal the extent to which KL modulates the ferrihydrite colloid transport, and (3) clarify in depth the interaction mechanisms between ferrihydrite colloids and KL.

2. Materials and methods

2.1. Ferrihydrite colloids, KL, and porous media

Ferrihydrite colloids were prepared following the method of Jasmine.[33] Briefly, 0.48 M $NaHCO_3$ (200 mL) was transferred with a peristaltic pump over ~50 min into 200 mL of 0.40 M $Fe(NO_3)_3\cdot 9H_2O$ that was being rapidly stirred by a magnetic stirrer and was held at 25 °C in a water bath. Once the transfer was completed, the mixture was heated in a microwave oven (950 W) until it boiled, and then it was quenched to room temperature in an ice bath. The suspension was dialyzed with a molecular weight membrane of 2 kDa against deionized (DI) water (18.2 MΩ cm) at 10 °C for 7 d to ensure that the supernatant conductivity was <5 μS cm^{-1} (nearly DI water). The final mixture was diluted ten-fold (1 g L^{-1}) and then stored in the dark (4 °C) for use.

Quartz sand (AR, 0.18–0.25 mm, Tianjin Kemiou Chemical Reagent Co., Ltd.) served as the model porous medium. Before use, it was pretreated to remove impurities (*e.g.*, clays, colloids, and metal oxides) on its surface. The quartz sand was soaked sequentially in 1 M NaOH and 1 M HNO_3 for 24 h each. It was then rinsed with DI water until the pH of the supernatant was constant, and dried at 105 °C for 24 h. KL ($Al_2O_7Si_2\cdot 2H_2O$) was purchased from Sigma-Aldrich. The KL-sand was prepared following previously published procedures.[28] The KL was treated with H_2O_2 to remove organic matter and gravity sedimentation was used to obtain particles with hydrodynamic diameter <2 μm. The KL suspensions (40 g L^{-1}) were flocculated with 50 mg L^{-1} polyvinyl alcohol, mixed for 30 min, and then centrifuged at 8000 rpm for 5 min. The quartz sand was added to the KL polymer complex slurry stirred for 15 min, dried at 80 °C for 24 h, then washed with DI water to remove excess KL and polyvinyl alcohol, and then dried again at 80 °C for 24 h.

2.2. Column experiments

Cylindrical Plexiglas columns (2.5 cm inner diameter × 10 cm length) were packed with cleaned quartz sand or KL-sand by applying the wet filling method to ensure saturation. The average pore volume (PV, 21.9 cm^3) and porosity (0.446) were determined from the volume of water filling the saturated sand column pore space. A peristaltic pump was used to upflow the pore solutions at 1 mL min^{-1} during the column experiments. Prior to use, the columns were equilibrated with 10 PVs of background solutions containing no ferrihydrite colloids. To study pH effects, the background solutions were made with different pH values (3.0, 4.0, 5.0, and 5.5) with 5 mM $NaNO_3$. To test the effects of ionic strength, the background solutions were set to 1, 5, and 10 mM $NaNO_3$ with pH 5.5. All the pH values of solutions were adjusted using 0.1 M HNO_3 or NaOH. Then each column received 17.33 PVs of ferrihydrite colloidal suspension (100 mg L^{-1}, stabilized in an ultrasonic bath for 30 min), followed by elution with 10 PVs of the ferrihydrite-free background solution. Effluent samples at the outlet of the column were collected using a fraction collector (collected in 10 mL glass vials every 7.30 min, nearly 0.33 PV). The light absorbance of the ferrihydrite colloid suspensions was measured at 420 nm using a UV–vis spectrophotometer (SHIMADZU, UV-2550), then converted to the ferrihydrite colloid concentration based on calibration curves (Fig. S1†).[34] The retention profile of the ferrihydrite colloids was also measured (details are shown in Section S1†). Each column was dismantled and divided into 10 sections (~1 cm long each) to collect sand or KL-sand under gravity. An acid digestion procedure was applied to dissolve the Fe(III) of the colloids retained on the sand or the KL-sand, and then the Fe concentration was measured using an atomic absorption spectrometer (PinAAcle 900T, PerkinElmer). The KBr solution (100 mg L^{-1}) was used as a nonreactive tracer to analyze the column hydrodynamic properties, and its concentration was measured with an ion chromatography system (Thermo Fisher Scientific).

2.3. Batch sorption experiments

For all the batch sorption experiments, the concentrations of $NaNO_3$ and the pH values were set based on the column experiments. KL was completely separated from the solutions after centrifugation (6000 rpm for 10 min), while the ferrihydrite colloids remained stable (not settled or adsorbed on the bottles). Thus, centrifugation was an effective method for separating ferrihydrite colloids from KL. The ferrihydrite colloids and KL were considered as the adsorbate and adsorbent, respectively.

Adsorption of ferrihydrite colloids on KL was conducted under ambient conditions (~25 °C). In the experiments, 100 mg of KL was put into 50 mL screw cap vials that already contained 30 mL ferrihydrite colloids suspensions (100 mg L^{-1}) with different concentrations of $NaNO_3$ and different pH values. For the adsorption kinetic experiment, the vials were shaken for 1, 5, 10, 15, 20, 25, 30, 35, 40, 50, 60, and 120 min, and then centrifuged at 6000 rpm for 10 min. The adsorption isotherm experiments were performed at different initial concentrations of ferrihydrite colloids of 50, 60, 70, 80, 90, and 100 mg L^{-1}. The vials were shaken for 2 h and then centrifuged. After centrifugation, the supernatant was used to determine the concentrations of the ferrihydrite colloids at 420 nm using a UV–vis spectrophotometer. The amount of adsorbed ferrihydrite colloids were then calculated by mass difference.

For desorption experiments, after removal of all the supernatants, 30 mL solutions of DI water containing the specified concentrations of $NaNO_3$ and pH values were added to the vials. The vials were then shaken for 2 h and recentrifuged, and the supernatants were measured for the desorbed colloids as described above. For ferrihydrite dissolution experiments, 30 mL of a citrate solution (1, 5, and 10 mM) was added to the vials, which were shaken and recentrifuged. Then the concentrations of colloids and Fe(III) in the supernatant were measured.

2.4. Characterization of colloidal particles adsorbed on KL

The crystallinity of the ferrihydrite colloids was determined with X-ray diffraction (XRD). The average hydrodynamic diameter of the ferrihydrite colloids and the zeta potential of the ferrihydrite colloids, sand, and KL in the batch experiments were measured with dynamic light scattering (DLS, Zetasizer Nano ZS90, Malvern). The specific surface area of the ferrihydrite was evaluated with the Brunauer–Emmett–Teller method (BET, ASAP 2460, MicroActive). The structure and morphology of the ferrihydrite colloids adsorbed on KL were observed under scanning electron microscopy (SEM, Merlin, ZEISS) with an energy dispersive X-ray spectroscopy (EDS) system and high-resolution transmission electron microscopy (HRTEM, Talos F200X, Thermo Fisher). The interaction mechanisms between the ferrihydrite colloids and KL were characterized by ITC and EXAFS (the details of ITC and EXAFS are provided in Section S2†).

2.5. Density functional theory (DFT) calculations

The Castep module of Material Studio 2020 was used to run the DFT calculations.[35–37] The generalized gradient approximation method with the Perdew–Burke–Ernzerhof function[38] was employed in the calculations to characterize the interactions between the ionic core and the valence electrons.[39,40] The energy cutoff of 450 eV was adopted for the plane-wave basis set. The Brillouin zone was sampled by employing a *k*-point of 1 × 1 × 1 for geometry optimization. The threshold values of the convergence criteria were specified as follows: 0.002 Å for the maximum displacement, 0.05 eV $Å^{-1}$ for the maximum force, 0.1 GPa for the maximum stress, 10^{-5} eV per atom for energy, and 2.0×10^{-6} eV per atom for self-consistent field tolerance. To eliminate the undesirable interactions between the molecules in the vacuum and the bottom side of the slab, a 20 Å vacuum space was implemented in the model. A (2 × 2) unit cell was employed to prevent the lateral interactions between molecules on the surface. A dimer of two Fe(III) octahedra was used as the model clusters of ferrihydrite. KL is a dioctahedral 1:1 type phyllosilicate clay mineral with a unit cell of $Al_4Si_4O_{10}(OH)_8$, and the (010) facet was chosen as an exemplary edge surface. The modelled structure of ferrihydrite and KL was assumed at the fully hydroxylated neutral surface. More information about the constructions of the KL and ferrihydrite models and the adsorption energy calculations are provided in Section S3.†

3. Results and discussion

3.1. Characterization of ferrihydrite colloids and KL-sand

Powder XRD was used to determine that the synthesized ferrihydrites were 6-line ferrihydrite (Fig. S2†). The HRTEM image (Fig. S3†) revealed that the average particle size of ferrihydrite colloids was 3–5 nm with uniform ellipsoid morphology, similar to those in previous reports.[41,42] The measured BET specific surface area of the ferrihydrite colloids was 309.2 $m^2\ g^{-1}$. The pH of the point of zero charge (pH_{PZC}) of the ferrihydrite colloids was determined to be ~8.3, which was in agreement with a previous report in the literature.[43] The average hydrodynamic diameter of the ferrihydrite colloids was measured in 100 mg L^{-1} solutions that were diluted from the stock suspension (10 g L^{-1}). The diameters were measured by DLS (Fig. S4†) and ranged from 42.3 to 65.9 nm at pH 3.0–5.5, which indicated that the ferrihydrite colloids remained relatively stable under these conditions. The aggregation became obvious when the pH was >6.0 (average hydrodynamic diameter >160 nm).

The SEM micrographs showed that the surface of the clean quartz sand was smooth and uniform (Fig. S5a†). The SEM images of the surface of the KL-sand composite showed numerous particles adhered to the sand (Fig. S5b†). The morphology of the particles on the quartz sand was consistent with that of pure KL (Fig. S5c†), which proved that KL was successfully attached to quartz sand without any morphological change. Moreover, the SEM-EDS spectra of the sand coated with KL showed prominent peaks of Si, Al, and O (Fig. S5d†), which indicated KL coverage on the quartz sand. The extent of coverage of KL on the quartz sand was estimated from the SEM images to be ~90% with a nonuniform distribution, which was similar to those reported previously.[23,28] The amount of KL coated on the sand was 9.86 ± 2.19 mg g^{-1}.

3.2. Effect of KL on ferrihydrite colloid transport

The column (sand and KL-sand) experiments were performed in this work to study the effect of KL on the migration of ferrihydrite colloids (Fig. 1). Br^- was used as an inert ion that was not retained in the quartz sand column, which began to appear at 1/3 PV and reached complete breakthrough at 1 PV (Fig. 1a and b). At pH = 3.0 and 5 mM $NaNO_3$, the initial breakthrough of ferrihydrite colloids occurred at 1 PV, and then reached a constant breakthrough after 2 PV, indicating that the sand column had an extremely slight retention effect on the ferrihydrite colloids. This conclusion was supported by the trace amount of ferrihydrite colloids retained in the sand column (Fig. 1c and d). However, the presence of KL was observed to have a distinct effect on the transport of ferrihydrite colloids (Fig. 1 and Table S1†). The effluent mass (M_{eff}) recovery of ferrihydrite colloids decreased from 96.9% to 73.8% when the KL was present under the conditions of pH = 3.0 and 5 mM $NaNO_3$ (Table S1†). Moreover, the M_{eff} of the ferrihydrite colloids in the KL-sand column decreased as the pH and $NaNO_3$ concentration increased (Table S1†). The KL also significantly altered the shape of the breakthrough curves and retention profiles of the ferrihydrite colloids, as shown in Fig. 1. Specifically, in the KL-sand column, the breakthrough of the ferrihydrite colloids was significantly delayed. The C/C_0 value (the ratio of the ferrihydrite colloid effluent concentration at a sampling time (C) to the ferrihydrite colloid influent concentration (C_0)) of ferrihydrite colloids remained zero during the first 4 PVs, and then increased slowly after 5 PVs, and achieved a steady-state breakthrough (C/C_0 was close to 1) at 13 PVs under the conditions of pH = 3.0 and 5 mM $NaNO_3$ (Fig. 1a). When the deposition sites of the surface of the sand were occupied, the migration of the ferrihydrite colloids was dominated by electrostatic repulsion, resulting in a significant breakthrough after 13 PVs.[14] The delay of the breakthrough curve of colloids was also reported in a previous study and the interaction between colloids and solid media was supposed to account for this phenomenon,[44] while the earlier breakthrough of colloids was found in another study when the interaction was minimal.[45] In present study, the interaction forces between KL and ferrihydrite colloids may account for a delayed breakthrough of colloids. The detailed mechanism of the interaction will be discussed later.

The retained ferrihydrite colloids maintained a relatively even distribution throughout the KL-sand column (Fig. 1c and d) because there was no aggregation of ferrihydrite colloids in the KL-sand column. Besides, aquifer materials have a limited colloid retention capacity, and the amount of available blocking sites reduced over time, and at last the deposition sites were completely occupied.[46] Similar breakthrough behavior for colloids on surface-modified porous media was previously observed.[19,23] Kuhnen *et al.* (2000) concluded that the complete breakthrough of ferrihydrite colloids on quartz sand was caused by the high electrostatic repulsion interactions between the particles and the particle-coated sand that created an energy barrier that inhibited the subsequent deposition.[47] The

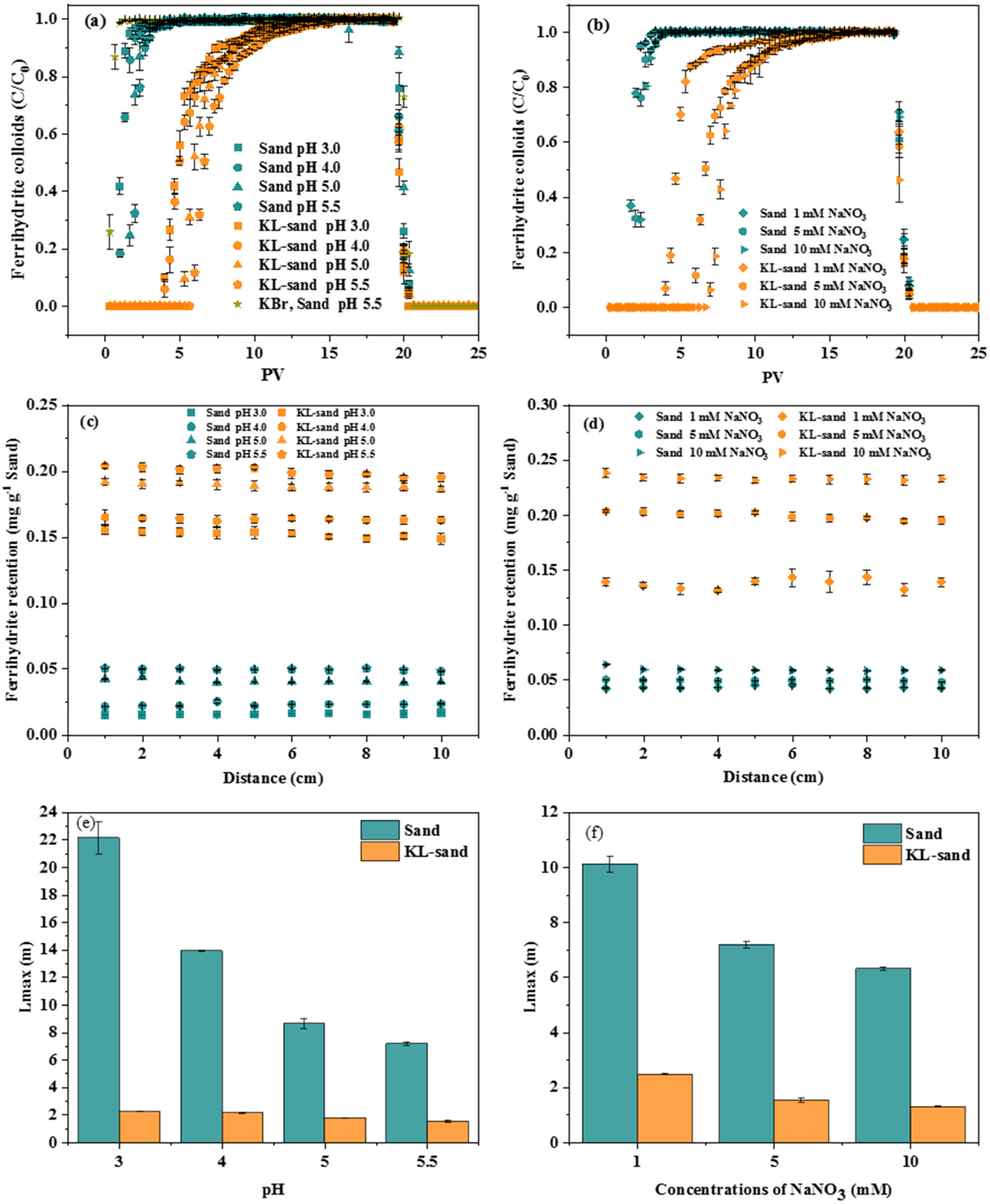

Fig. 1 Breakthrough curves of ferrihydrite colloids at different pH levels (a) and $NaNO_3$ concentrations (b). Retention profiles of ferrihydrite colloids at different pH levels (c) and $NaNO_3$ concentrations (d). Predicted maximum travel distance of ferrihydrite colloids at different pH levels (e) and concentrations of $NaNO_3$ (f). C/C_0 is the ratio of the ferrihydrite colloid effluent concentration at a sampling time (C) to the ferrihydrite colloid influent concentration.

breakthrough of ferrihydrite colloids in the KL-sand column was slightly delayed at higher pH values and $NaNO_3$ concentrations, which might be a result of the increased electrostatic attraction interactions between the ferrihydrite colloids and the KL-sand (Fig. 1a and b). In our experiments, the amount of ferrihydrite colloids retained in the KL-sand column was 3.14–9.29 times higher than that in the sand column. This may be due to the absorption of ferrihydrite colloids by KL.

To further evaluate the effect of KL on the transport of ferrihydrite colloids, the maximum transport distance ($L_{\max}$), which is the distance over which 99.9% of the particles are retained in the medium, was calculated using colloid filtration theory:[48]

$$L_{\max} = -\frac{2}{3}\frac{d_c}{(1-\theta)\alpha\eta_0}\ln(M_{\mathrm{eff}})$$

where d_c is the diameter of the medium (sand or KL-sand), θ is the porosity of the column, α is the attachment efficiency, and η_0 is the single-collector contact efficiency. The detailed calculation method is shown in Section S4.† The presence of KL led to high deposition rate coefficients (k_d = 2.1–4.0 × 10^{-4} s^{-1}) and low transport distances ($L_{\max} < 2.5$ m) of ferrihydrite colloids in the column under all our experimental conditions (Table S1†). The $L_{\max}$ of ferrihydrite colloids in the absence of KL was nearly 4.1–9.8 times larger than that in the presence of KL (Fig. 1e and f). This may be attributed to the KL providing more deposition sites for the ferrihydrite colloids.[22] The specific mechanism of the interaction between KL and the ferrihydrite colloids will be discussed later.

3.3. Adsorption–desorption behaviors of ferrihydrite colloids on KL

Pure KL was evaluated for its adsorption ability for ferrihydrite colloids. Pseudo-first-order[49] and pseudo-second-order equations[50] were usually applied to explain the adsorption performance of solute sorption on the sorbent. We try to employ them to analyze the adsorption behavior of colloids. Time-dependent adsorption curves of ferrihydrite colloids on KL at different pH levels and $NaNO_3$ concentrations are shown in Fig. 2a and b, respectively. It was clearly seen that KL sorbed ferrihydrite colloids instantaneously over 30 min and slowed until approaching the equilibrium state within 240 min (Fig. 2a and b). The experimental data for ferrihydrite colloid adsorption on KL were fitted well by the pseudo-second-order equation (Table S2†), which indicated that a relatively rapid chemical interaction took place on the KL.[51] The fit to the data determined that the adsorption capacity and rate constant of the ferrihydrite colloids were 19.3 mg g^{-1} and 0.197 mg g^{-1} min^{-1}, respectively, at pH 5.5 and 5 mM $NaNO_3$ (Table S2†).

Adsorption isotherms of the ferrihydrite colloids were also generated at pH 5.5 and 5 mM $NaNO_3$ concentration to further understand the adsorption behavior on the KL. The experimental results showed that the maximum ferrihydrite colloid adsorption capacity was 19.8 mg g^{-1} for KL (Fig. 2c). The relationship between KL and ferrihydrite colloid concentration at equilibrium was fitted with three two-parameter isotherm models (Langmuir, Freundlich, and Temkin) and two three-

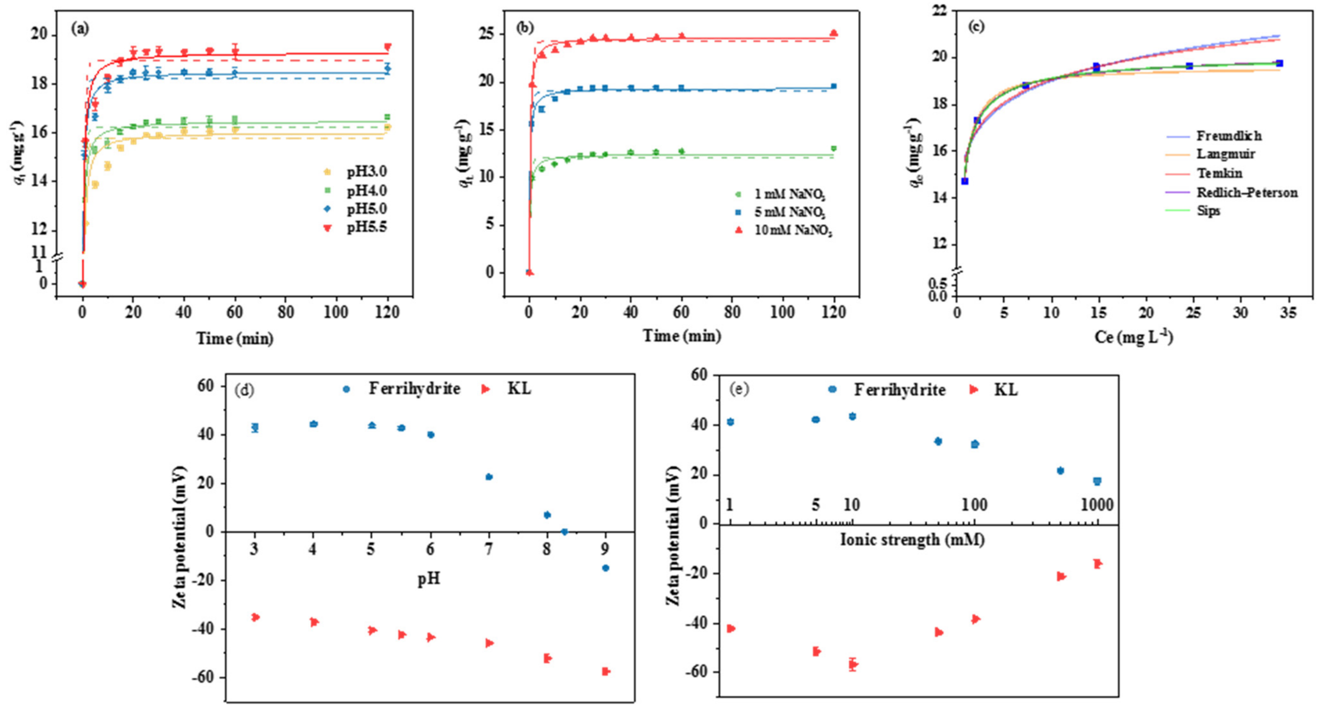

Fig. 2 Adsorption of ferrihydrite colloids on KL as a function of time at different pH levels (a) and $NaNO_3$ concentrations (b), and the corresponding fitting results of the pseudo-first-order equation (broken line) and the pseudo-second-order equation (full line). The ferrihydrite colloid adsorption isotherms and the corresponding fitting results of the adsorption isotherm models (Freundlich, Langmuir, Temkin, Redlich–Peterson and Sips) (c). The zeta potential of ferrihydrite colloids and KL at different pH levels (d) and $NaNO_3$ concentrations (e).

parameter adsorption isotherm models (Redlich–Peterson and Sips).[52,53] The detailed characteristics and formula of these models are presented in Section S5. The fitting results are presented in Fig. 2c and Table S3.† Of the two-parameter models, the Langmuir model was more suitable to describe ferrihydrite colloid adsorption features on KL. Both of the three-parameter models provided fit the experimental data accurately. The value of β of the Redlich–Peterson isotherm approached 1, meaning that the Redlich–Peterson isotherm converged with the Langmuir isotherm.[53] These fitting results indicated that monolayer chemical adsorption occurred on the KL surface,[54,55] which was supported by the SEM observations (Fig. 3f). Based on the Sips model, the maximum capacity of the ferrihydrite colloids adsorbed on the KL was 20.2 mg g^{-1}, which matched the experimental data and showed that this adsorption isotherm model was applicable to explain the sorption behavior of ferrihydrite nanoparticles on the sorbent.

To determine the influence of pH on the adsorption of ferrihydrite colloids on KL, the adsorption edges were analyzed at pH levels of 3.0–5.5 (Fig. 2a). The ferrihydrite colloid adsorption capacities of KL raised from 16.3 to 19.5 mg g^{-1} with increased pH from 3.0 to 5.5, showing that the adsorption behavior of ferrihydrite colloids exhibited pH-dependence. As shown in Fig. 2d, the zeta potential of ferrihydrite colloids was positive when the solution pH was below 8.3,[43] while the zeta potential of KL was negative.[20] Therefore, the electrostatic attraction interactions between the KL surface and the ferrihydrite colloids might significantly affect the quantity of adsorbed ferrihydrite colloids.[56,57] The effects of ionic strength (1, 5, and 10 mM $NaNO_3$) on the adsorption of ferrihydrite colloids on KL were also examined. When the concentration of $NaNO_3$ increased from 1 to 10 mM, the equilibrium adsorption of ferrihydrite colloids on the KL increased from 13.0 to 25.2 mg g^{-1} (Fig. 2b). The zeta potential of ferrihydrite colloids remained relatively stable when the $NaNO_3$ concentration increased from 1 to 10 mM, and the zeta potential of KL significantly decreased (Fig. 2e). Therefore, the trend of the zeta potential curve was correlated with the adsorption of ferrihydrite colloids on the KL particles with increasing pH and $NaNO_3$ concentration, suggesting that the electrostatic interaction likely determined the adsorption behavior. Zhao *et al.* (2015) found that goethite could adsorb and remove graphene oxide from solutions due to the electrostatic interactions between the positively charged goethite and the negatively charged graphene oxide,[34] which was consistent with the work presented here. These results explained the migration behavior of ferrihydrite colloids in the column containing KL-sand at different pH values and ionic strengths, which further indicated that the mass transfer of ferritic colloids was affected by their adsorption on KL.

Desorption of ferrihydrite colloids from KL was also investigated. There were no ferrihydrite colloids detected in the supernatant when the pH value or ionic strength was changed (Fig. S6a and b†), indicating that this ferrihydrite colloid fraction was unable to desorb from KL (irreversible adsorption). In the case of protein adsorption on the titanium surface, this interception was also viewed as irreversible adsorption due to the formation of chemical bonds.[58] The surface complexation method has been widely

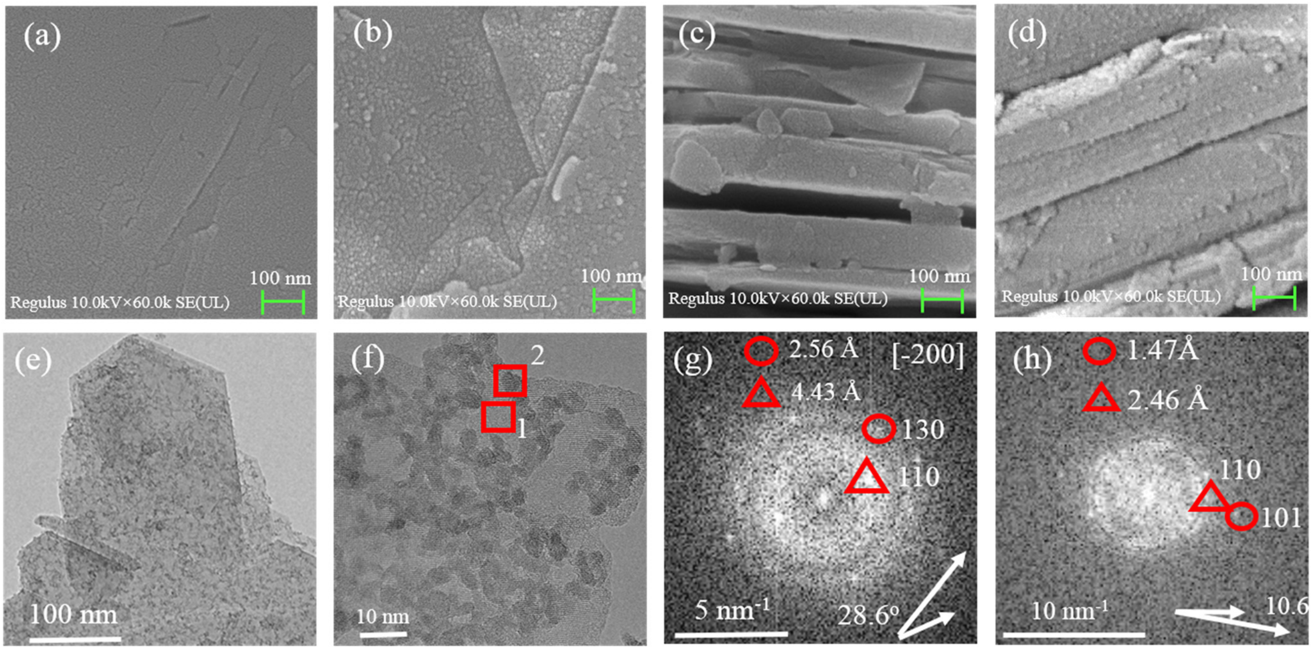

Fig. 3 SEM images of the normal KL surface (a) and the layered KL surface (c), and ferrihydrite colloids adsorbed on the normal KL surface (b) and the layered KL surface (d). TEM micrograph (e) and selected area electron diffraction images (f) of the complexes of ferrihydrite colloids adsorbed on KL. The fast Fourier transform of areas 1 (g) and 2 (h) in (f).

used for the dissolution of many minerals.[59] For example, organic acids have been shown to enhance the dissolution of Fe(III) oxides by forming surface complexes.[60] Hofmann *et al.* (2007) determined that the release and transport of ferrihydrite colloids in a sand column are affected by citrate, and their results showed that both the repulsive interfacial forces and bond breaking at the ferrihydrite colloids–quartz sand interface (the dissolution of ferrihydrite) controlled the ferrihydrite colloids' breakthrough.[61] In the present study, the release of ferrihydrite colloids adsorbed on KL was explored using citrate at different concentrations (1, 5, and 10 mM). Free Fe(III) was detected in the desorption solution but no ferrihydrite colloids were detected (Fig. S6c and d†), which indicated that the dissolution of ferrihydrite had a controlling role in the release of ferrihydrite colloids from KL. The dissolution rate and amount of ferrihydrite colloids increased as the citrate concentration increased, and nearly total dissolution was achieved after 30 h at 10 mM citrate. These results suggested that ferrihydrite colloids may be primarily chemically bonded to KL.

3.4. The morphology characterization of KL and ferrihydrite colloid complexes

Reversible deposition of ferrihydrite colloids on quartz sand was observed by Liang *et al.*, 2000,[62] indicating that the irreversibility of ferrihydrite colloid adsorption on KL was related to the specific particle–particle configuration.[34] Therefore, the configuration of KL and ferrihydrite colloid complexes was further investigated. SEM images showed that KL had a smooth surface and layered structure (Fig. 3a and c), which was consistent with previous studies.[63,64] When KL and ferrihydrite colloids were both present, a number of fine particles appeared on the KL surface (Fig. 3b and d), suggesting that many ferrihydrite colloids were adsorbed on the surface of KL. Moreover, the SEM-EDS spectra of the KL sample with adsorbed ferrihydrite colloids contained prominent peaks corresponding to Fe, which also showed that ferrihydrite colloids covered the KL surface (Fig. S7a†). In HRTEM images, the ferrihydrite colloids appeared as many spherical solids, 3–5 nm in size, on the KL, and the ferrihydrite colloids did not aggregate together on the KL surface (Fig. 3e and f). These results agreed with the fitted result of the adsorption isotherm models that indicated a monolayer ferrihydrite colloid adsorption on the KL surface. Fig. 3g and h show the corresponding fast Fourier transform images of areas 1 and 2, respectively, in Fig. 3f. In Fig. 3g, the interplanar spacings were 2.56 and 4.43 Å, corresponding to the (130) and (110) crystal planes of KL. In Fig. 3h, the interplanar spacings were 1.47 and 2.46 Å, corresponding to the (101) and (110) crystal planes of ferrihydrite, indicating that there were no phase transitions after adsorption of ferrihydrite colloids on KL. In addition, the result of the TEM-EDS analysis showed that there were significantly higher peaks of Fe in area 2 than in area 1 (Fig. S7b†), which further proved that the spherical solids were ferrihydrite colloids. Fig. S8† shows that ferrihydrite colloids did not completely and uniformly cover the KL. In conclusion, phase transitions or agglomeration did not occur after the ferrihydrite colloids adsorbed on KL and were not the cause of the irreversible adsorption of the ferrihydrite colloids on the KL.

3.5. Thermodynamic characterization of interfacial reactions

For small organic molecules, the formation of chemical bonds is usually used to explain the desorption hysteresis of adsorbents.[65,66] To improve the understanding of adsorption mechanisms and to determine whether there are chemical bonds between ferrihydrite colloids and KL, the binding behavior of ferrihydrite colloids and KL was thermodynamically characterized with ITC, as shown in Fig. 4. Adsorption of ferrihydrite colloids on KL was exothermic with a ΔH value of -85.1 kJ mol^{-1}. The entropy of the adsorption of ferrihydrite colloids and KL was positive (190.2 J mol^{-1} K^{-1}), suggesting a random increase at the ferrihydrite colloid–sorbent interface.[67] Inner-sphere complexes form with positive entropies because the solvating water molecules are expelled from the surface adsorption sites during surface complexation, leading to an increase in disorder.[68,69] Consequently, the inner-sphere complexation was probably the main mechanism of ferrihydrite colloid adsorption on KL. These thermodynamic results are consistent with those predicted by the adsorption kinetics and isotherm models, indicating that the models used to explain the adsorption mechanism of solute sorption onto the sorbent were also applicable to express the mechanism of ferrihydrite nanoparticle adsorption onto the KL.

3.6. Local coordination environments of ferrihydrite colloids on the KL surface

3.6.1. EXAFS spectroscopy analysis. EXAFS spectroscopy was employed to analyze the Fe interfacial species and molecular structures on the KL surfaces. The EXAFS spectra fitting results (Fig. S9 and Table S4†) showed that the first peak represented six oxygen atoms bound to a central Fe at an average distance of 1.95 Å for ferrihydrite and 1.97 Å for ferrihydrite adsorbed on KL. Optimized fits to features at a greater distance caused by Fe backscatter corresponded to average Fe–Fe interatomic distances of 3.02 and 3.24 Å for ferrihydrite (Fig. S9a and Table S4†). The ferrihydrite-containing KL sample had a second shell peak, which could be fitted with Al/Si or Fe as the backscattering atom, with Fe–Fe interatomic distances of 3.04 and 3.29 Å and Fe–Al/Si interatomic distances of 3.02 and 3.28 Å (Fig. S9b and c†). Differentiating the Al and Si atoms based on backscattering amplitudes was not possible due to the juxtaposition of Si and Al in the periodic table.[70] Analysis of the Fe K-edge in the EXAFS spectra provided the average Fe–Fe distances, from which the Fe–Al distances could not be distinguished, which agreed with observations in previous work.[71] Compared with pure ferrihydrite, the Fe–Fe distance of the composite sample increased slightly. Previous studies revealed that in the sample of Al-substituted hematite, when there was more Al substitution the Fe and Al atoms were closer, leading to a

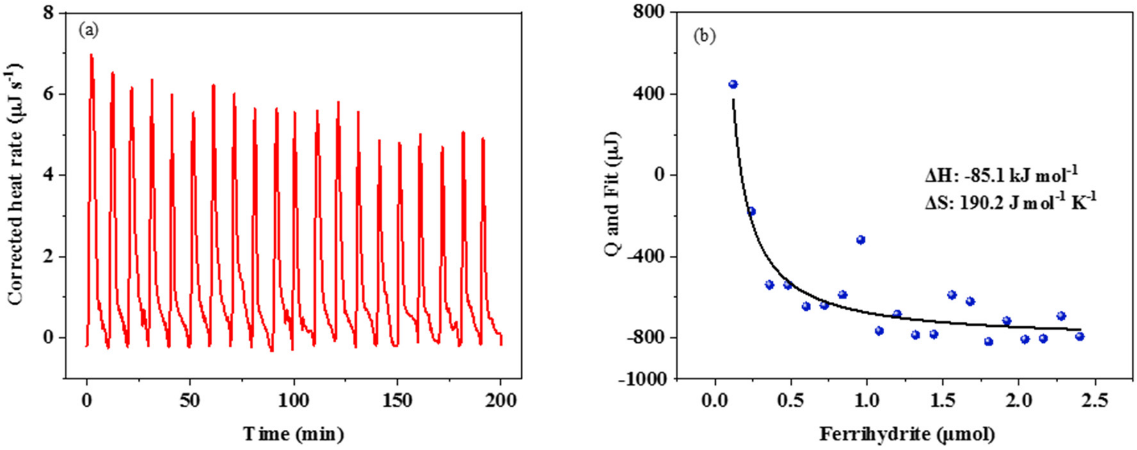

Fig. 4 (a) Calorimetric titrations (corrected heat rate) and (b) integrated heat values for the addition of ferrihydrite colloids to KL. The full line represents the best independent model fitting results.

decrease in the Al–Fe bond distance and an increase in the adjacent Fe–Fe bond distances.[71,72] Therefore, ferrihydrite could coordinate to Al and Si sites on the KL surface. Moreover, the obtained Fe–Al/Si interatomic distances (3.02 and 3.28 Å) indicated that ferrihydrite formed inner-sphere surface complexes with KL.

3.6.2. Periodic model calculations. The structure of the adsorbed ferrihydrite–KL interface was also analyzed with periodic model calculations (Fig. 5). The energy of adsorption (E_{ads}) was usually employed to estimate the adsorption affinity, with a more negative E_{ads} representing a stronger adsorption affinity.[73] The E_{ads} values of the formed complexes were calculated and are summarized in Table S5.† For adsorption on an Al octahedral sheet, three coordination modes were established to investigate the adsorbed ferrihydrite structures. The geometry-optimized periodic models are presented in Fig. 5a–c. Of the one bidentate complex and two monodentate complexes that were modeled, only one of the monodentate complexes was exothermic. A monodentate mononuclear complex was bound with E_{ads} = 7.05 eV, and the bidentate mononuclear structure was bound with E_{ads} = 6.49 eV, indicating that these two configurations

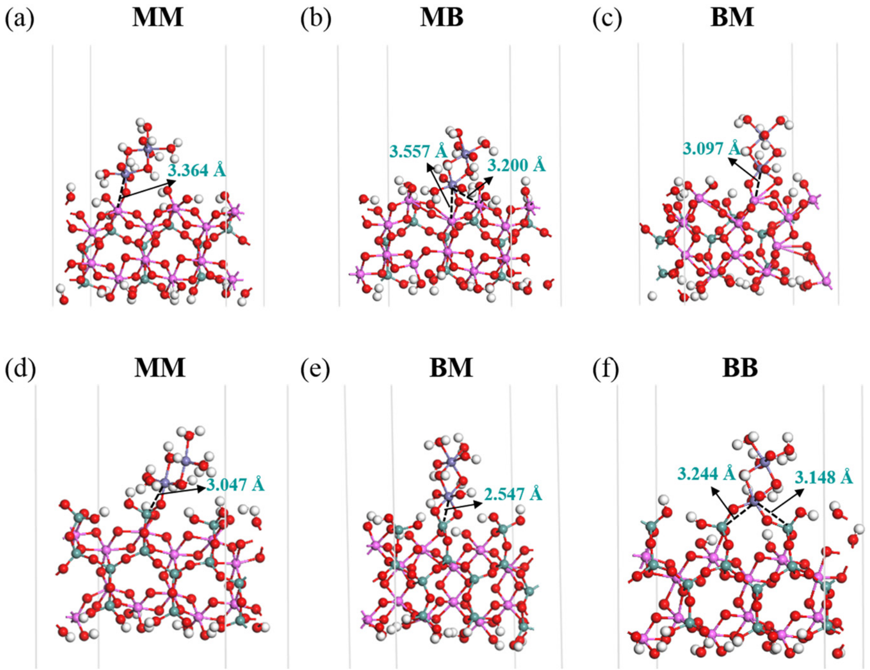

Fig. 5 Geometry-optimized periodic models of ferrihydrite adsorption on the Al octahedral sheet and Si tetrahedral sheets of KL. The complex of MM (a), MB (b), and BM (c) on the Al octahedral sheet; the complex of MM (d), BM (e) and BB (f) on the Si tetrahedral sheet. The red, purple, pink, cyan and white spheres represent oxygen, iron, aluminum, silicon, and hydrogen atoms, respectively. MM: monodentate mononuclear; MB: monodentate binuclear; BM: bidentate mononuclear; BB: bidentate binuclear.

were unstable structures. The monodentate binuclear complex had a lower E_{ads} (−0.03 eV), indicating that this complex had good thermodynamic stability. For adsorption on the Si tetrahedral sheet (Fig. 5d–f), the bidentate mononuclear and bidentate binuclear configurations were endothermic, with E_{ads} of 5.83 and 5.31 eV, respectively, making them relatively unstable configurations. The monodentate mononuclear configuration was exothermic with $E_{\text{ads}} = -3.48$ eV, which indicated the greatest stability. Therefore, ferrihydrite adsorbed on KL as a monodentate coordination rather than a bidentate coordination, based on both the Al octahedral and Si tetrahedral sheets.

The adsorption configurations of the surface complexes could also be determined by comparing the interatomic distances.[51] The distances between Fe and the adjacent Al or Si atoms, as well as the lengths of the Fe–O, Al–O, and Si–O bonds, are listed in Table S6.† The average Fe–Al interatom distance for the monodentate binuclear complexes was 3.37 ± 0.18 Å, which agreed well with EXAFS spectroscopy results (3.02–3.28 Å). A previous study also stated that Fe (hydr) oxides and KL can bind together *via* Fe–O–Al/Si bonds.[31] Although the bidentate mononuclear Fe–Al and bidentate binuclear Fe–Si interatomic distances of 3.10 and 3.15–3.24 Å, respectively, were also close to the results of the above EXAFS spectroscopy, their E_{ads} suggested that they were relatively unstable configurations. Moreover, the Fe–Si interatomic distance of the monodentate mononuclear configuration (3.05 Å) more closely matched the results of the EXAFS analysis, indicating that the monodentate mononuclear complex on the Si tetrahedral sheet was the dominant species on the KL. These results further suggested that the monodentate mononuclear complex on the Si tetrahedral sheet and the monodentate binuclear complex on the Al octahedral sheet are the thermodynamically favored adsorption structures on KL. Compared with the previous study that speculated the interaction mechanism of goethite and KL,[31] the present study clarified the interaction mechanism of ferrihydrite and KL in the molecular-scale, and evidence was provided to identify that inner-sphere complexation was included in the interaction of KL and ferrihydrite.

4. Conclusions

The present study demonstrated that the KL-coated sand column significantly inhibits the migration of ferrihydrite colloids. This inhibition was mainly ascribed to KL's high adsorption capacity for ferrihydrite colloids (20.2 mg g^{-1}), which was due to electrostatic interactions. The ferrihydrite colloids could not be desorbed from KL (irreversible adsorption), but could be released from KL by dissolving with citrate. The results of ITC revealed that ferrihydrite colloids adsorb onto KL *via* an exothermic process, and the main adsorption mechanism was forming inner-sphere complexes. Moreover, it was further confirmed by EXAFS and DFT calculations that ferrihydrite colloids coordinated to the surfaces of KL *via* the monodentate inner-sphere complex with high thermodynamic stability. These results offer new understanding into the role of KL in the migration of ferrihydrite colloids, which are critical for understanding the movement of ferrihydrite colloids and their associated contaminants in natural soils and aquatic environments.

Conflicts of interest

The authors declare no competing financial interest.

Acknowledgements

This study was supported by National Natural Science Foundation of China (No. 41931288 and 42277238) and Guangdong Natural Science Foundation (No. 2023A1515012128).

References

1 J. N. Ryan and M. Elimelech, Colloid mobilization and transport in ground-water, *Colloids Surf., A*, 1996, **107**, 1–56.

2 G. Bin, X. D. Cao, Y. Dong, Y. M. Luo and L. Q. Ma, Colloid deposition and release in soils and their association with heavy metals, *Crit. Rev. Environ. Sci. Technol.*, 2011, **41**(4), 336–372.

3 R. Celis, M. C. Hermosin, L. Cox and J. Cornejo, Sorption of 2,4-dichlorophenoxyacetic acid by model particles simulating naturally occurring soil colloids, *Environ. Sci. Technol.*, 1999, **33**, 1200–1206.

4 C. E. Martinez and M. B. McBride, Dissolved and labile concentrations of Cd, Cu, Pb, and Zn in aged ferrihydrite-organic matter systems, *Environ. Sci. Technol.*, 1999, **33**, 745–750.

5 R. Kretzschmar, M. Borkovec, D. Grolimund, M. Elimelech and D. L. Sparks, Mobile subsurface colloids and their role in contaminant transport, *Adv. Agron.*, 1999, **66**, 121–193.

6 T. K. Sen and K. C. Khilar, Review on subsurface colloids and colloid-associated contaminant transport in saturated porous media, *Adv. Colloid Interface Sci.*, 2006, **119**, 71–96.

7 Y. J. Zhang, J. L. Guo, J. C. Xue, C. L. Bai and Y. Guo, Phthalate metabolites: Characterization, toxicities, global distribution, and exposure assessment, *Environ. Pollut.*, 2021, **291**, 118106.

8 A. A. Porubcan and S. Xu, Colloid straining within saturated heterogeneous porous media, *Water Res.*, 2011, **45**(4), 1796–1806.

9 J. Won and S. E. Burns, Role of immobile kaolinite colloids in the transport of heavy metals, *Environ. Sci. Technol.*, 2018, **52**, 2735–2741.

10 D. Grolimund, M. Borkovec, K. Barmettler and H. Sticher, Colloid-facilitated transport of strongly sorbing contaminants in natural porous media: A laboratory column study, *Environ. Sci. Technol.*, 1996, **30**(10), 3118–3123.

11 S. Chotpantarat and N. Kiatvarangkul, Facilitated transport of cadmium with montmorillonite KSF colloids under different pH conditions in water-saturated sand columns: Experiment and transport modeling, *Water Res.*, 2018, **146**, 216–231.

12 J. Won, X. Wirth and S. E. Burns, An experimental study of cotransport of heavy metals with kaolinite colloids, *J. Hazard. Mater.*, 2019, **373**, 476–482.

13 R. Piazza, Settled and unsettled issues in particle settling, *Rep. Prog. Phys.*, 2014, **77**(5), 056602.

14 P. Liao, S. H. Yuan and D. J. Wang, Impact of redox reactions on colloid transport in saturated porous media: an example of ferrihydrite colloids transport in the presence of sulfide, *Environ. Sci. Technol.*, 2016, **50**, 10968–10977.

15 O. S. Alimi, J. F. Budarz, L. M. Hernandez and N. Tufenkji, Microplastics and nanoplastics in aquatic environments: Aggregation, deposition, and enhanced contaminant transport, *Environ. Sci. Technol.*, 2018, **52**(4), 1704–1724.

16 C. Jin, S. D. Normani and M. B. Emelko, Surface roughness impacts on granular media filtration at favorable deposition conditions: Experiments and modeling, *Environ. Sci. Technol.*, 2015, **49**(13), 7879–7888.

17 D. T. Lin, L. M. Hu, S. A. Bradford, X. H. Zhang and I. M. C. Lo, Simulation of colloid transport and retention using a pore-network model with roughness and chemical heterogeneity on pore surfaces, *Water Resour. Res.*, 2021, **57**(2), e2020WR028571.

18 P. Liao, C. Pan, W. Y. Ding, W. L. Li, S. H. Yuan, J. D. Fortner and D. E. Giammar, Formation and transport of Cr(III)-NOM-Fe colloids upon reaction of Cr(VI) with NOM-Fe(II) colloids at anoxic-oxic interfaces, *Environ. Sci. Technol.*, 2020, **54**(7), 4256–4266.

19 Z. S. Rastghalam, C. R. Yan, J. Y. Shang and T. Cheng, The role of Fe oxyhydroxide coating, illite clay, and peat moss in nanoscale titanium dioxide (nTiO(2)) retention and transport in geochemically heterogeneous media, *Environ. Pollut.*, 2020, **257**, 113625.

20 J. Y. Wu, Q. Y. Ye, P. X. Wu, S. R. Xu, Y. J. Liu, Z. Ahmed, S. Rehman and N. W. Zhu, Heteroaggregation of nanoplastics with oppositely charged minerals in aquatic environment: Experimental and theoretical calculation study, *Chem. Eng. J.*, 2022, **428**, 131191.

21 H. J. Kim, T. Phenrat, R. D. Tilton and G. V. Lowry, Effect of kaolinite, silica fines and pH on transport of polymer-modified zero valent iron nano-particles in heterogeneous porous media, *Adv. Colloid Interface Sci.*, 2012, **370**, 1–10.

22 X. Y. Ye, Z. Cheng, M. Wu, Y. R. Hao, G. P. Lu, B. X. Hu, C. H. Mo, Q. S. Li, J. F. Wu and J. C. Wu, Effects of clay minerals on the transport of polystyrene nanoplastic in groundwater, *Water Res.*, 2022, **223**, 118978.

23 X. Q. Yin, Y. J. Jiang, Y. H. Tan, X. M. Meng, H. M. Sun and N. Wang, Co-transport of graphene oxide and heavy metal ions in surface-modified porous media, *Chemosphere*, 2019, **218**, 1–13.

24 T. T. Chen and L. J. Cabri, Mineralogical overview of iron control in hydrometallurgical processing, in *Conference of Iron Control in Hydrometallurgy*, ed. J. E. Dutrizac and A. J. Monhemius, 1986, pp. 19–55.

25 J. L. Jambor and J. E. Dutrizac, Occurrence and constitution of natural and synthetic ferrihydrite, a widespread iron oxyhydroxide, *Chem. Rev.*, 1998, **98**, 2549–2586.

26 F. M. Michel, L. Ehm, S. M. Antao, P. L. Lee, P. Chupas, G. Liu, D. R. Strongin, M. A. A. Schoonen, B. L. Phillips and J. B. Parise, The structure of ferrihydrite, a nanocrystalline material, *Science*, 2007, **316**(5832), 1726–1729.

27 A. Navrotsky, L. Mazeina and J. Majzlan, Size-driven structural and thermodynamic complexity in iron oxides, *Science*, 2008, **319**, 1635.

28 J. Jerez and M. Flury, Humic acid-, ferrihydrite-, and aluminosilicate-coated sands for column transport experiments, *Colloids Surf., A*, 2006, **273**, 90–96.

29 Y. L. Sun, D. Q. Pan, X. Y. Wei, D. F. Xian, P. Wang, J. J. Hou, Z. Xu, C. L. Liu and W. S. Wu, Insight into the stability and correlated transport of kaolinite colloid: Effect of pH, electrolytes and humic substances, *Environ. Pollut.*, 2020, **266**, 115189.

30 T. Schafer, F. Huber, H. Seher, T. Missana, U. Alonso, M. Kumke, S. Eidner, F. Claret and F. Enzmann, Nanoparticles and their influence on radionuclide mobility in deep geological formations, *Appl. Geochem.*, 2012, **27**(2), 390–403.

31 S. Y. Wei, W. F. Tan, F. Liu, W. Zhao and L. P. Weng, Surface properties and phosphate adsorption of binary systems containing goethite and kaolinite, *Geoderma*, 2014, **213**, 478–484.

32 T. Hiemstra, Ferrihydrite interaction with silicate and competing oxyanions: Geometry and hydrogen bonding of surface species, *Geochim. Cosmochim. Acta*, 2018, **238**, 453–476.

33 J. J. Erbs, B. Gilbert and R. L. Penn, Influence of Size on Reductive Dissolution of Six-Line Ferrihydrite, *J. Phys. Chem. C*, 2008, **112**(32), 12127–12133.

34 J. Zhao, F. Liu, Z. Wang, X. Cao and B. Xing, Heteroaggregation of Graphene Oxide with Minerals in Aqueous Phase, *Environ. Sci. Technol.*, 2015, **49**, 2849–2857.

35 M. D. Segall, P. J. D. Lindan, M. J. Probert, C. J. Pickard, P. J. Hasnip and S. J. Clark, Firstprinciples simulation: Ideas, illustrations and the CASTEP code, *J. Phys.: Condens. Matter*, 2002, **14**, 2717–2744.

36 Y. H. Han, W. L. Liu and J. H. Chen, DFT simulation of the adsorption of sodium silicate species on kaolinite surfaces, *Appl. Surf. Sci.*, 2016, **370**, 403–409.

37 L. Song, W. Liu, F. Xin and Y. Li, Study of adhesion properties and mechanism of sodium silicate binder reinforced with silicate fume, *Int. J. Adhes. Adhes.*, 2021, **106**(13), 102820.

38 J. P. Perdew, K. Burke and M. Ernzerhof, Generalized gradient approximation made simple, *Phys. Rev. Lett.*, 1996, **77**, 3865–3868.

39 D. Vanderbilt, Soft self-consistent pseudopotentials in a generalized eigenvalue formalism, *Phys. Rev. B: Condens. Matter Mater. Phys.*, 1990, **4**, 7892–7895.

40 A. E. Gen, A. Aka and B. Kutlu, The catalytic effect of the Au(111) and Pt(111) surfaces to the sodium borohydride hydrolysis reaction mechanism: A DFT study, *Int. J. Hydrogen Energy*, 2018, **6**, 1–13.

41 X. M. Wang, W. Li, R. Harrington, F. Liu, J. B. Parise, X. H. Feng and D. L. Sparks, Effect of ferrihydrite crystallite size

on phosphate adsorption reactivity, *Environ. Sci. Technol.*, 2013, **47**, 10322–10331.

42 L. Y. He, L. Xie, D. J. Wang, W. L. Li, J. D. Fortner, Q. Q. Li, Y. H. Duan, Z. Q. Shi, P. Liao and C. X. Liu, Elucidating the Role of Sulfide on the Stability of Ferrihydrite Colloids under Anoxic Conditions, *Environ. Sci. Technol.*, 2019, **53**, 4173–4184.

43 P. Liao, W. L. Li, D. J. Wang, Y. Jiang, C. Pan, J. D. Fortner and S. H. Yuan, Effect of reduced humic acid on the transport of ferrihydrite nanoparticles under anoxic conditions, *Water Res.*, 2017, **109**, 347–357.

44 C. V. Chrysikopoulos and V. E. Katzourakis, Colloid particle size-dependent dispersivity, *Water Resour. Res.*, 2015, **51**, 4668–4683.

45 S. Sasidharan, S. Torkzaban, S. A. Bradford, P. J. Dillon and P. G. Cook, Coupled effects of hydrodynamic and solution chemistry on long-term nanoparticle transport and deposition in saturated porous media, *Colloids Surf., A*, 2014, **457**, 169–179.

46 F. J. Leij, S. A. Bradford, Y. Wang and A. Sciortino, Langmuirian Blocking of Irreversible Colloid Retention: Analytical Solution, Moments, and Setback Distance, *J. Environ. Qual.*, 2015, **44**, 1473–1482.

47 F. Kuhnen, K. Barmettler, S. Bhattacharjee, M. Elimelech and R. Kretzschmar, Transport of iron oxide colloids in packed quartz sand media: Monolayer and multilayer deposition, *J. Colloid Interface Sci.*, 2000, **231**(1), 32–41.

48 N. Tufenkji and M. Elimelech, Correlation equation for predicting single-collector efficiency in physicochemical filtration in saturated porous media, *Environ. Sci. Technol.*, 2004, **38**(2), 529–536.

49 Y. S. Ho and G. Mckay, A comparison of chemisorption kinetic models applied to pollutant removal on various sorbents, *Process Saf. Environ. Prot.*, 1998, **76**(4), 332–340.

50 Y. S. Ho and G. Mckay, Pseudo-second order model for sorption processes, *Process Biochem.*, 1999, **34**, 451–465.

51 X. Li, C. Guo, X. Jin, Q. Yao, Q. Liu, L. Zhang, G. Lu, J. R. Reinfelder, W. Huang and Z. Dang, Molecular-scale study of Cr(VI) adsorption onto lepidocrocite facets by EXAFS, in situ ATR-FTIR, theoretical frequency calculations and DFT+U techniques, *Environ. Sci.: Nano*, 2022, **9**, 568–581.

52 A. Gunay, E. Arslankaya and I. Tosun, Lead removal from aqueous solution by natural and pretreated clinoptilolite: Adsorption equilibrium and kinetics, *J. Hazard. Mater.*, 2007, **146**, 362–371.

53 A. B. Perez-Marin, V. M. Zapata, J. F. Ortuno, M. Aguilar, J. Saez and M. Llorens, Removal of cadmium from aqueous solutions by adsorption onto orange waste, *J. Hazard. Mater.*, 2007, **139**, 122–131.

54 A. Sari, M. Tuzen, D. Citak and M. Soylak, Equilibrium, kinetic and thermodynamic studies of adsorption of Pb(II) from aqueous solution onto Turkish kaolinite clay, *J. Hazard. Mater.*, 2007, **149**(2), 283–291.

55 D. Zhang, J. X. Liu, S. B. Zhu, H. X. Xiong and Y. Q. Xu, Adsorption removal of Cr(VI) by isomeric FeOOH, *Water Sci. Technol.*, 2019, **80**, 300–307.

56 M. J. Wang, Q. Zhang, T. T. Lu, J. Y. Chen, Q. Q. Wei, W. F. Chen, Y. M. Zhou and Z. C. Qi, Colloid-mediated transport of tetracycline in saturated porous media: Comparison between ferrihydrite and montmorillonite, *J. Environ. Manage.*, 2021, **299**, 113638.

57 K. Zhao, S. Tufail, Y. Arai, P. Sharma, Q. R. Zhang, Y. H. Chen, X. Wang and J. Y. Shang, Effect of phytic acid and morphology on Fe (oxyhydr)oxide transport under saturated flow condition, *J. Hazard. Mater.*, 2022, **424**, 127659.

58 K. Imamura, M. Shimomura, S. Nagai, M. Akamatsu and K. Nakanishi, Adsorption characteristics of various proteins to a titanium surface, *J. Biosci. Bioeng.*, 2008, **106**, 273–278.

59 A. E. Blum and A. C. Lasaga, The role of surface speciation in the dissolution of minerals, *Nature*, 1988, **331**, 431–433.

60 T. D. Waite and F. M. M. Morel, Photoreductive dissolution of colloidal iron oxide in natural waters, *Environ. Sci. Technol.*, 1984, **18**, 860–868.

61 A. Hofmann and L. Liang, Mobilization of colloidal ferrihydrite particles in porous media - An inner-sphere complexation approach, *Geochim. Cosmochim. Acta*, 2007, **71**(24), 5847–5861.

62 L. Y. Liang, A. Hofmann and B. H. Gu, Ligand-induced dissolution and release of ferrihydrite colloids, *Geochim. Cosmochim. Acta*, 2000, **64**(12), 2027–2037.

63 M. T. Ding, H. Su, K. Yang, Y. Li, F. F. Li and B. Xue, Preparation and characterization of an aluminosilicate material with layer expansion structure, *Appl. Clay Sci.*, 2021, **211**, 106179.

64 Y. Y. Zhang, Y. Y. Luo, X. Q. Yu, D. F. Huang, X. T. Guo and L. Y. Zhu, Aging significantly increases the interaction between polystyrene nanoplastic and minerals, *Water Res.*, 2022, **219**, 118544.

65 K. Yang and B. S. Xing, Desorption of polycyclic aromatic hydrocarbons from carbon nanomaterials in water, *Environ. Pollut.*, 2007, **145**, 529–537.

66 J. Zhao, Z. Wang, Q. Zhao and B. Xing, Adsorption of phenanthrene on multi-layer graphene as affected by surfactant and exfoliation, *Environ. Sci. Technol.*, 2014, **48**, 331–339.

67 H. Du, W. Chen, P. Cai, X. Rong, X. Feng and Q. Huang, Competitive adsorption of Pb and Cd on bacteriaemontmorillonite composite, *Environ. Pollut.*, 2016, **218**, 168–175.

68 D. Gorman-Lewis, J. B. Fein and M. P. Jensen, Enthalpies and entropies of proton and cadmium adsorption onto Bacillus subtilis bacterial cells from calorimetric measurements, *Geochim. Cosmochim. Acta*, 2006, **70**, 4862–4873.

69 L. C. Fang, Q. Y. Huang, X. Wei, W. Liang, X. M. Rong, W. L. Chen and P. Cai, Microcalorimetric and potentiometric titration studies on the adsorption of copper by extracellular polymeric substances (EPS), minerals and their composites, *Bioresour. Technol.*, 2010, **101**, 5774–5779.

70 M. Gräfe, B. Singh and M. Balasubramanian, Surface speciation of Cd(II) and Pb(II) on kaolinite by XAFS spectroscopy, *J. Colloid Interface Sci.*, 2007, **315**, 21–32.

71 W. Li, X. L. Liang, P. F. An, X. H. Feng, W. F. Tan, G. H. Qiu, H. Yin and F. Liu, Mechanisms on the morphology variation

of hematite crystals by Al substitution: The modification of Fe and O reticular densities, *Sci. Rep.*, 2016, **6**, 35960.

72 Y. Zhang, Electronegativities of elements in valence states and their applications. 1. Electronegativities of elements in valence states, *Chem. Inf.*, 1983, 14.

73 S. Qiu, H. S. Yan, X. H. Qiu, H. Wu, X. W. Zhou, H. Q. Wu, X. B. Li and T. S. Qiu, Adsorption of La on kaolinite (001) surface in aqueous system: A combined simulation with an experimental verification, *J. Mol. Liq.*, 2022, **347**, 117956.